Salazar et al. Supplemental Figure 1

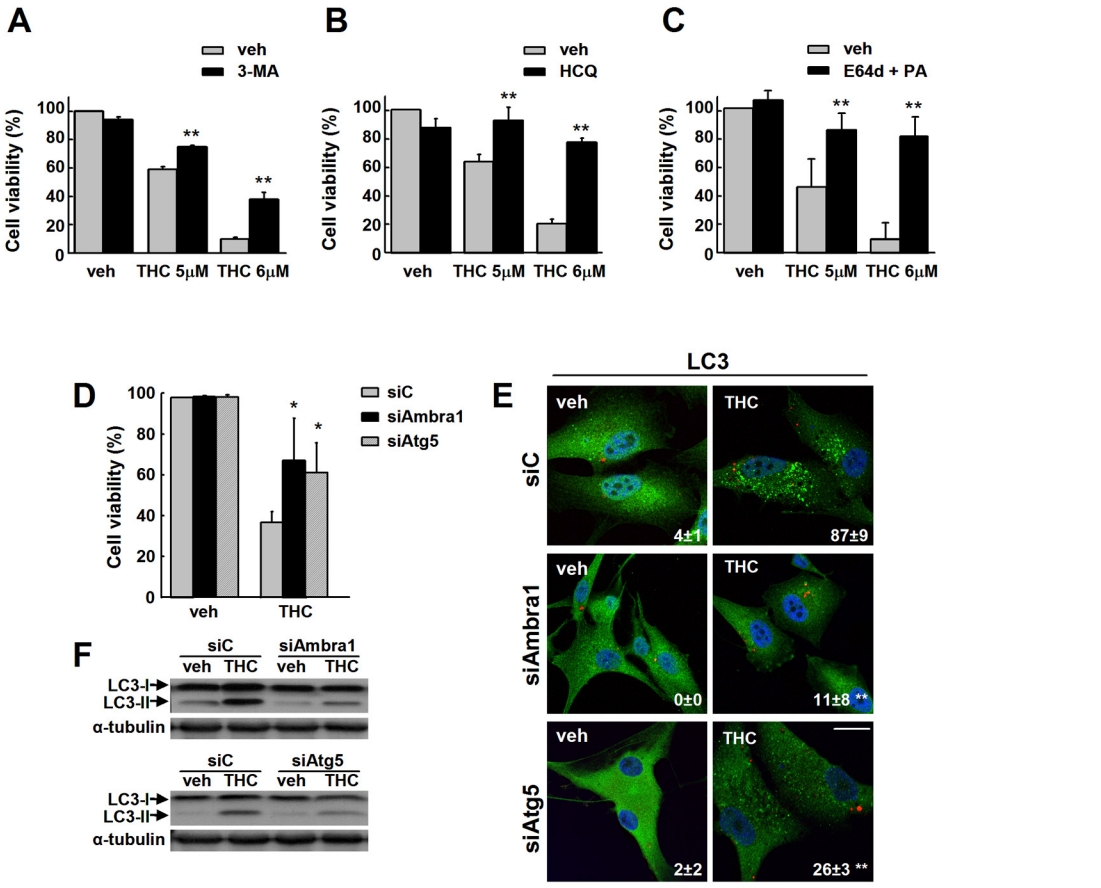

Supplemental Figure 1

Pharmacological and genetic inhibition of autophagy prevents THC-induced cell death. (**A-C**): Effect of THC (24 h) on the viability of U87MG cells pre-incubated with vehicle or 3-MA (5 mM; **A**), hydroxicloroquine (HCQ; 15 μg/ml; **B**) and E64d + PA (10 μM +10 μg/ml; **C**) (mean ± s.d.; n = 10; $*P < 0.05$ or $**P < 0.01$ from THC-treated cells). (**D**) Effect of THC (24 h) on the viability of U87MG cells transfected with siC, siAmbra1 or siAtg5 (mean ± s.d.; n = 5; $*P < 0.05$ from THC-treated siC-transfected cells). Values of gene expression as determined by real-time quantitative PCR (expressed as mean fold change ± s.d. relative to siC-transfected cells; n = 5; $**P < 0.01$ from siC-transfected cells) were 0.3 ± 0.1** and 0.4± 0.1** for siAmbra1- and siAtg5-transfected cells, respectively. (**E**) Effect of THC (18 h) on LC3 immunostaining (green) in U87MG cells transfected with siC, siAmbra1 or siAtg5. Values represent the percentage of cells with LC3 dots relative to the total number of transfected cells (as determined by co-transfection with a red fluorescent control siRNA) (mean ± s.d.; n = 4; $**P < 0.01$ from THC-treated siC-transfected cells). Bar: 20 μm. (**F**) Effect of THC (18 h) on LC3 lipidation in U87MG cells transfected with siC, siAmbra1 or siAtg5 (n = 5).

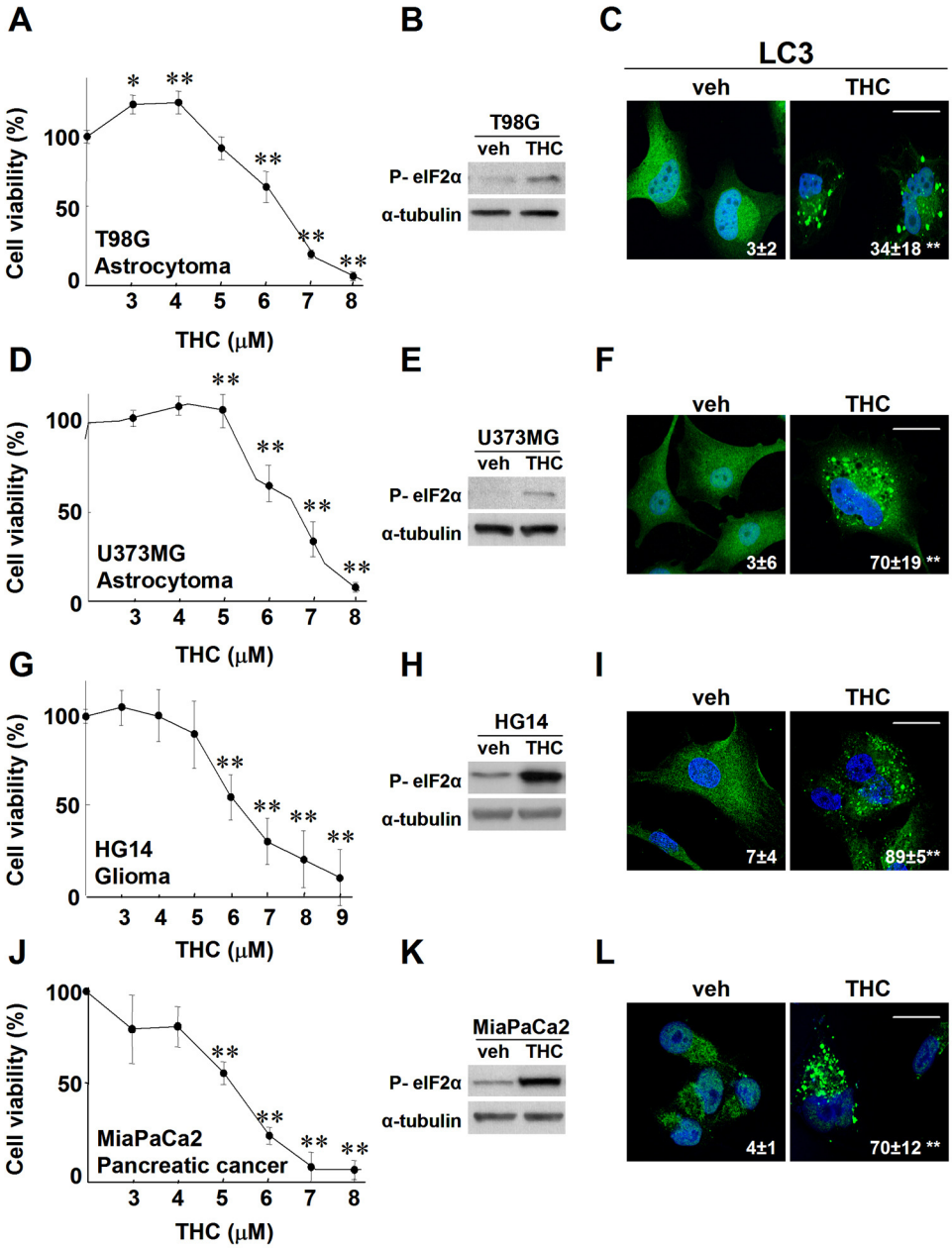

Supplemental Figure 2
THC induces ER-stress, autophagy and cell death in human tumor cells. (**A, D, G. J**) Effect of THC on the viability of T98G (**A**, astrocytoma), U373MG (**D**, astrocytoma), HG14 (**G**, a primary culture derived from a human glioblastoma biopsy), and MiaPaCa2 (**J**, pancreatic cancer) cells (mean ± s.d.; n = 10; **P* < 0.05 or ***P* < 0.01 from vehicle-treated cells). (**B, E, H, K**) Effect of THC on eIF2α phosphorylation of T98G (**B**), U373MG (**E**), HG14 (**H**) and MiaPaCa2 (**K**) cells (3 h; n = 3). (**C, F, I, L**) Effect of THC (18 h) on LC3 immunostaining of T98G (**C**), U373MG (**F**), HG14 (**I**), and MiaPaCa2 (**L**) cells. Values represent the percentage of cells with LC3 dots relative to the total number of cells (mean ± s.d.; n = 3; ***P* < 0.01 from vehicle-treated cells). Bar: 20 μm.

Salazar et al. Supplemental Figure 3

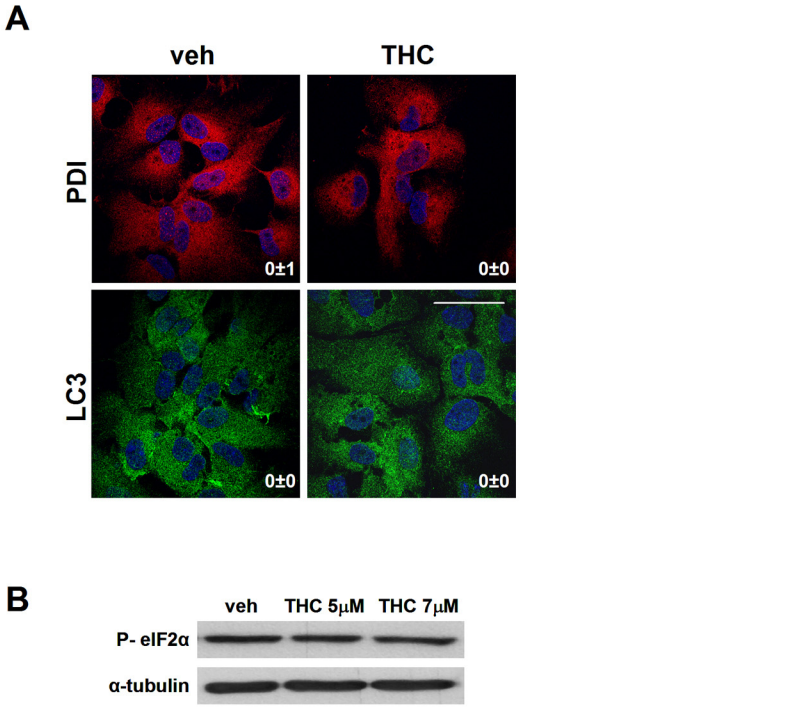

Supplemental Figure 3
Primary astrocytes are resistant to THC-induced ER-stress and autophagy. (**A**) Effect of THC on PDI (8 h) and LC3 (24 h) immunostaining of primary astrocytes (n = 3). Values represent the percentage of cells with PDI (upper photomicrographs) or LC3 (lower photomicrographs) dots relative to the total number of cells (mean ± s.d.; n = 3). Bar: 20 μm. (**B**) Effect of THC on eIF2α phosphorylation of primary astrocytes (3 h; n = 3).

Salazar et al. Supplemental Figure 4

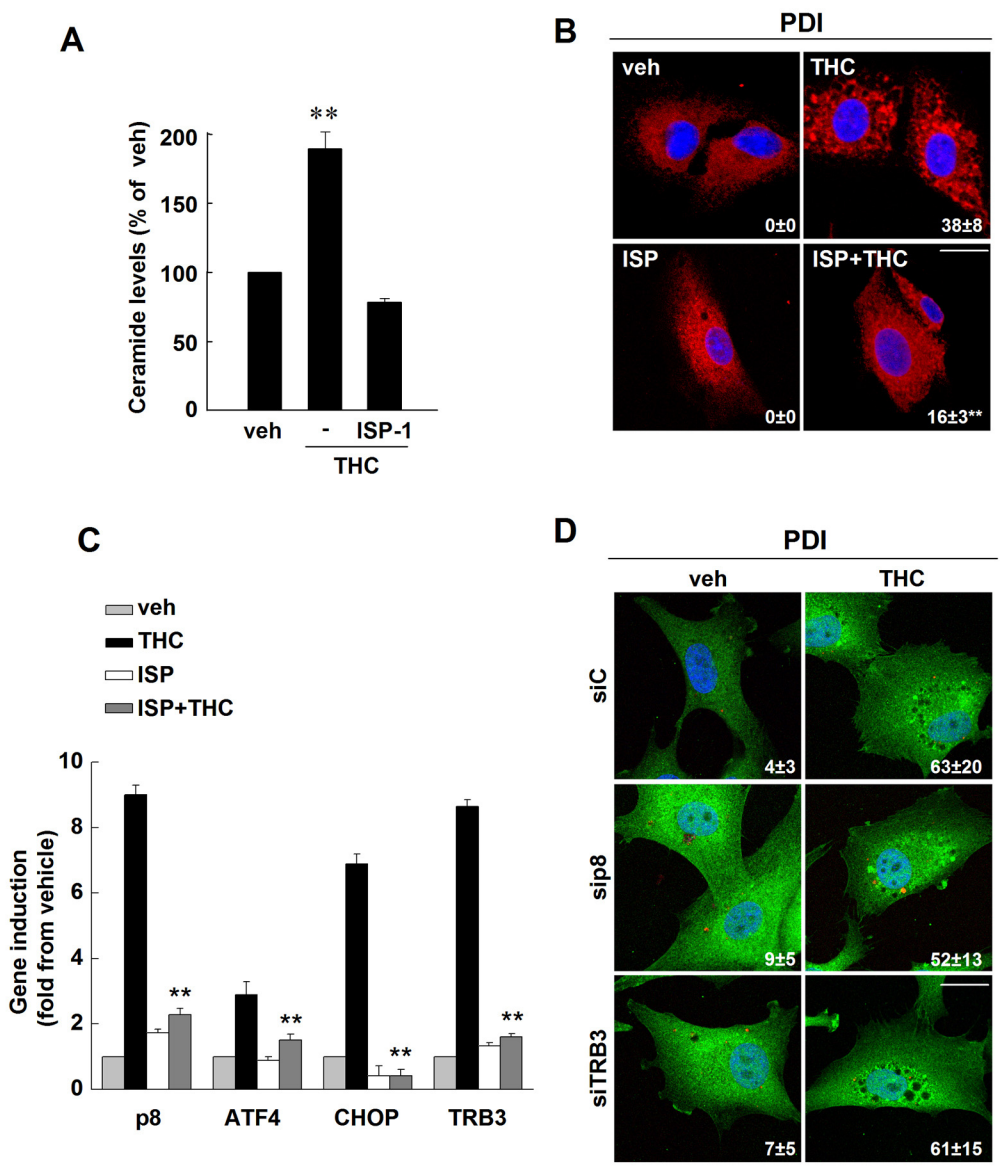

Supplemental Figure 4
Inhibition of ceramide biosynthesis but not knock-down of p8 or TRB3 prevents THC-induced ER dilation. (**A**) Effect of THC (8 h) on ceramide levels of U87MG cells pre-incubated with vehicle or ISP-1 (1 μM) (mean ± s.d.; n = 3; $^{**}P < 0.01$ from vehicle-treated cells). (**B**) Effect of THC on PDI immunostaining (red) of U87MG cells preincubated with ISP-1 (1 μM) (6 h; n = 3). Values represent the percentage of cells with PDI dots relative to the total number of cells (mean ± s.d.; n = 3; $^{**}P < 0.01$ from THC-treated cells). Bar: 20 μm. (**C**) Effect of THC (8 h) on p8, ATF-4, CHOP and TRB3 mRNA levels of U87MG pre-treated with vehicle or ISP-1 (1 μM). Data are expressed as the mean fold-increase ± s.d. relative to vehicle-treated cells. (n = 6; $^{**}P < 0.01$ from THC-treated cells). (**D**) Effect of THC (8 h) on PDI immunostaining (green) of U87MG cells transfected with control (siC), p8 (sip8) or TRB3 (siTRB3) -selective siRNA. Values represent the percentage of cells with PDI dots relative to the total number of transfected cells (as determined by co-transfection with a red fluorescent control siRNA) (mean ± s.d.; n = 4). Bar: 20 μm.

Salazar et al. Supplemental Figure 5

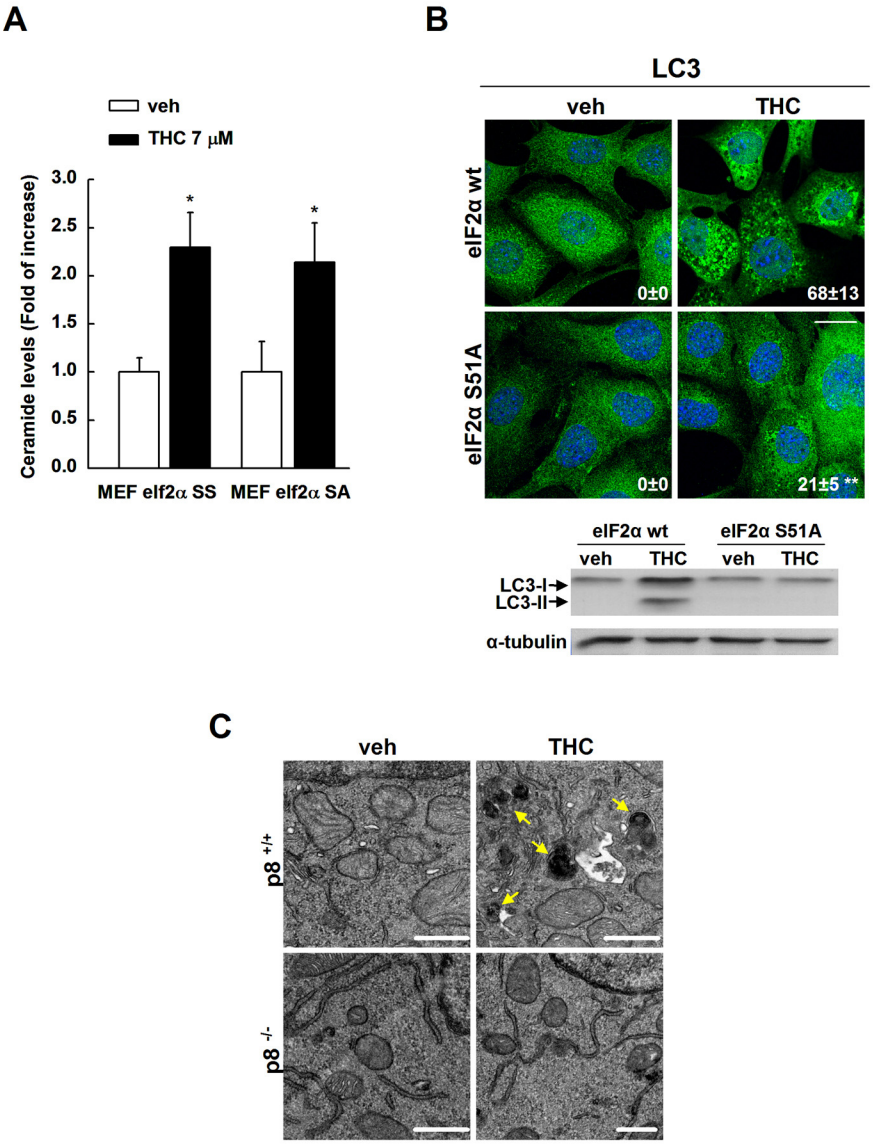

Supplemental Figure 5
eIF2α S51A and p8$^{-/-}$ MEFs are resistant to THC-induced autophagy. (**A**) Effect of THC (8 h) on ceramide levels of eIF2α wt and S51A MEFs. (mean ± s.d.; n = 3; *P < 0.05 from vehicle-treated cells) (**B**) Upper panel: Effect of THC (18 h) on LC3 immunostaining of eIF2α wt and S51A MEFs. Values represent the percentage of cells with LC3 dots relative to the total number of cells (mean ± s.d.; n = 4; **P < 0.01 from THC-treated eIF2α wt MEFs). Bar: 20 μm. Lower panel: Effect of THC (18 h) on LC3 lipidation of eIF2α wt and S51A MEFs (n = 3). (**C**) Effect of THC (6 h) on p8$^{+/+}$ and p8$^{-/-}$ MEFs. Representative electron microscopy photomicrographs are shown. Note the presence of late autophagosomes in p8$^{+/+}$ THC but not vehicle (veh)-treated cells (arrows). Bars: 500 nm.

Salazar et al. Supplemental Figure 6

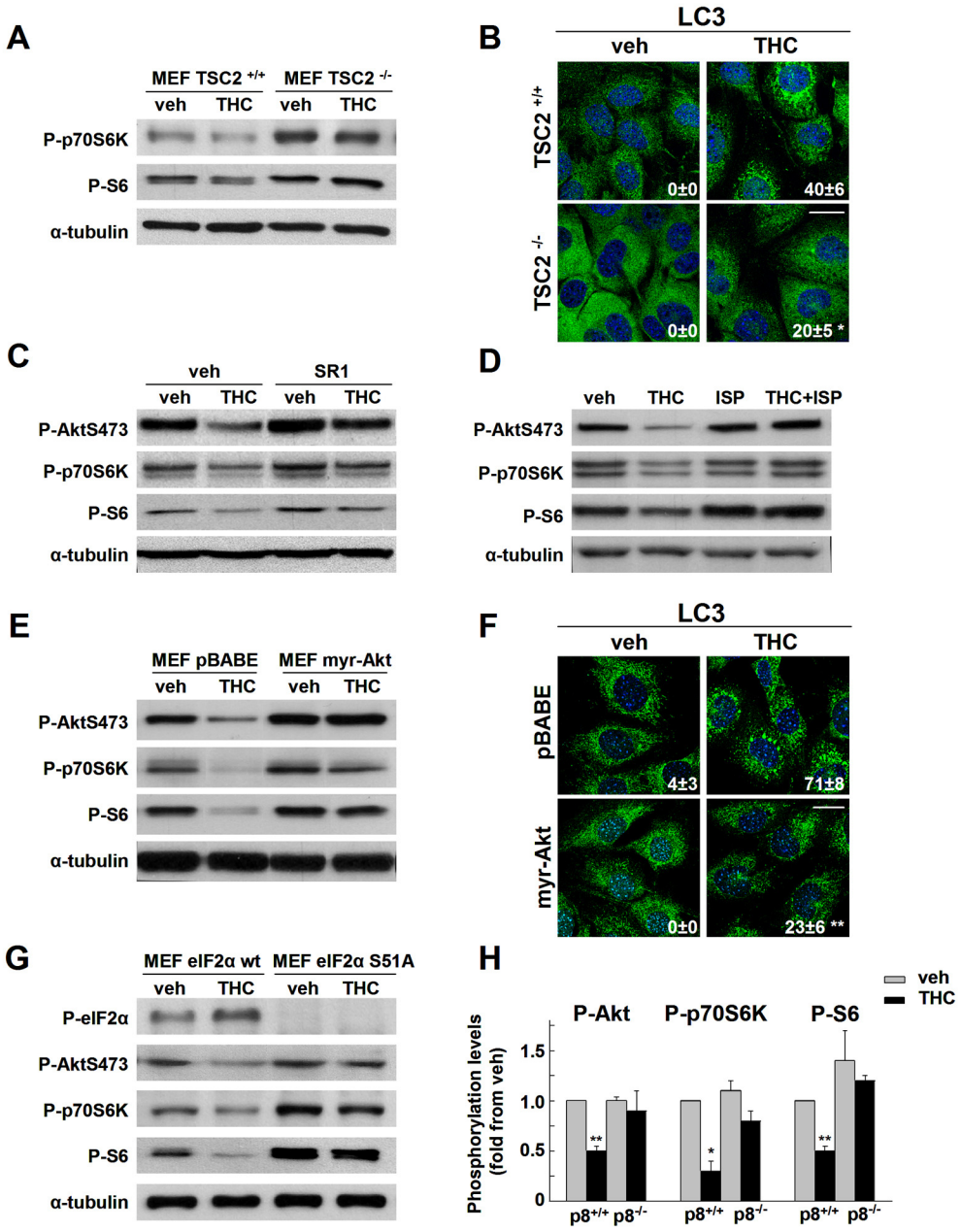

Supplemental Figure 6

TSC2$^{-/-}$, myr-Akt, eIF2α S51A and p8$^{-/-}$ MEFs as well as SR1- or ISP-1-treated U87MG cells are resistant to THC-induced mTORC1 inhibition. (**A**) Effect of THC (18 h) on p70S6k and S6 phosphorylation of TSC2$^{+/+}$ and TSC2$^{-/-}$ MEFs (n = 3). (**B**) Effect of THC (18 h) on LC3 immunostaining of TSC2$^{+/+}$ and TSC2$^{-/-}$ MEFs. Values represent the percentage of cells with LC3 dots relative to the total number of cells (mean ± s.d.; n = 3; $^{**}P < 0.01$ from THC-treated TSC2$^{+/+}$ MEFs). Bar: 20 μm. (**C**) Effect of THC (18 h) on Akt, p70S6k and S6 phosphorylation of U87MG cells pre-incubated with vehicle or SR1 (1 μM; n = 3). (**D**) Effect of THC (18 h) on Akt, p70S6k and S6 phosphorylation of U87MG cells pre-incubated with vehicle or ISP-1 (1 μM; n = 3). (**E**) Effect of THC (18 h) on Akt, p70S6k and S6 phosphorylation of pBABE and myr-Akt MEFs (n = 4). (**F**) Effect of THC (18 h) on LC3 immunostaining of pBABE and myr-Akt MEFs. Values represent the percentage of cells with LC3 dots relative to the total number of cells (mean ± s.d.; n = 3; $^{**}P < 0.01$ from THC-treated pBABE MEFs). Bar: 20 μm. (**G**) Effect of THC on eIF2α (3 h), Akt, p70S6k and S6 (18 h) phosphorylation of eIF2α wt and S51A MEFs (n = 5). (**H**) Effect of THC (18 h) on Akt, p70S6k and S6 phosphorylation of p8$^{+/+}$ and p8$^{-/-}$. Data represent the optical density values relative to vehicle-treated p8$^{+/+}$ MEFs (mean ± s.d.; n = 7; $^{*}P < 0.05$ or $^{**}P < 0.01$ from vehicle-treated p8$^{+/+}$ MEFs).

Salazar et al. Supplemental Figure 7

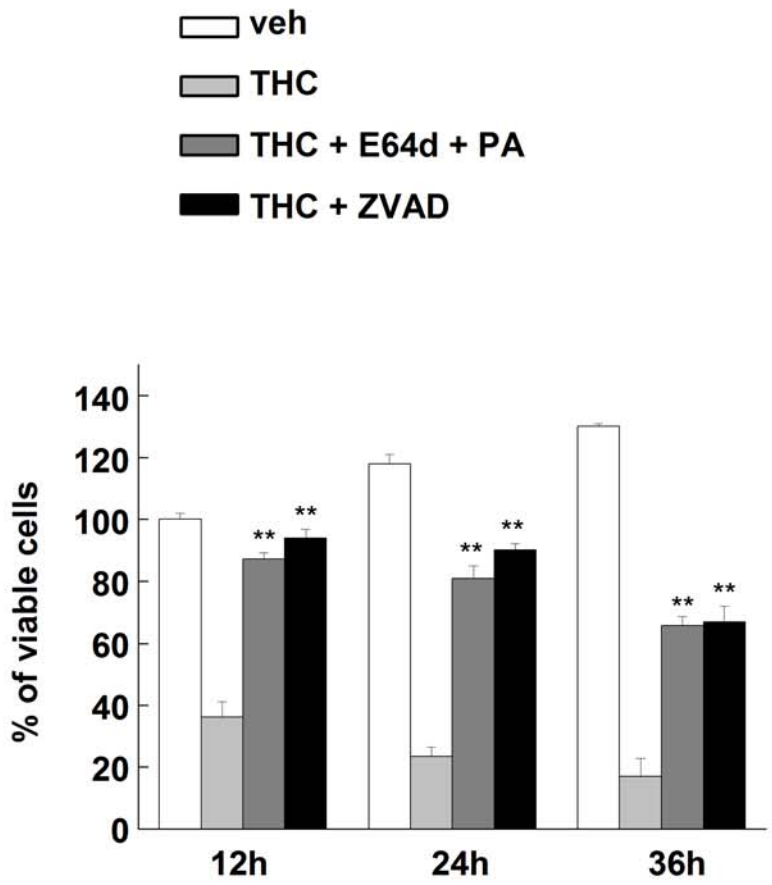

Supplemental Figure 7
Pharmacological inhibition of autophagy or apoptosis prevents THC-induced cell death. Effect of THC on the viability of U87MG cells pre-incubated with vehicle, E64d + pepstatine A (PA) (10 μM + 10 μg/ml) or ZVAD (10 μM) (mean ± s.d.; n = 3; $^{**}P < 0.01$ from THC-treated cells). Data are expressed as the percentage of viable cells relative to 12 h vehicle-treated cells.

Salazar et al. Supplemental Figure 8

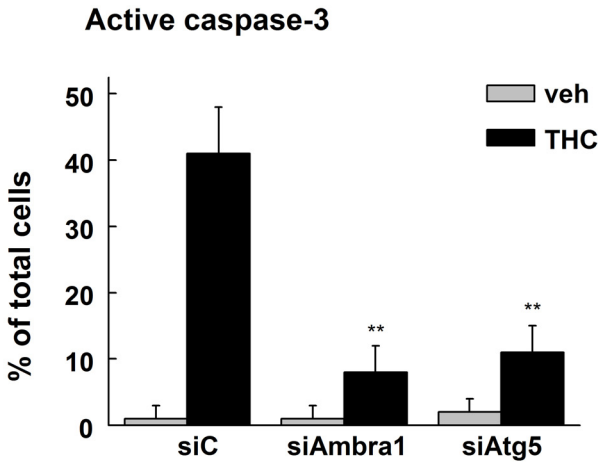

Supplemental Figure 8
Genetic inhibition of autophagy prevents THC-induced apoptosis. Effect of THC (24 h) on active caspase-3 immunostaining of U87MG cells transfected with siC, siAmbra1 or siAtg5. Data represent the percentage of active caspase-3 positive cells relative to the total number of transfected cells (as determined by co-transfection with a red fluorescent control siRNA) (mean ± s.d.; n = 3; $^{**}P < 0.01$ from THC-treated siC-transfected cells).

Salazar et al. Supplemental Figure 9

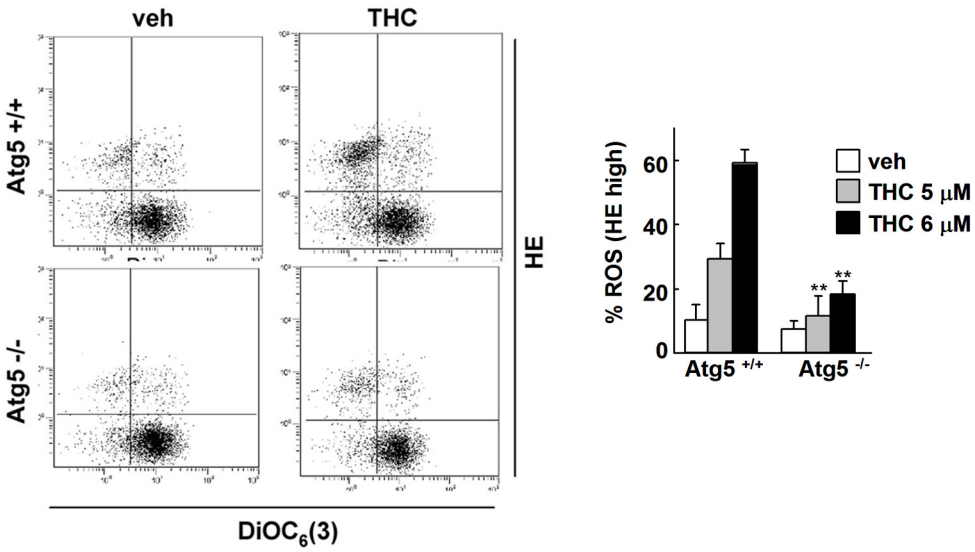

Supplemental Figure 9
Autophagy is upstream of apoptosis in THC-induced cell death. Effect of THC (24 h) on loss of mitochondrial membrane potential and ROS production of $Atg5^{+/+}$ and $Atg5^{-/-}$ MEFs as determined by $DIOC_6(3)$ and HE cytofluorometric analysis. A representative dot plot experiment is shown. Data represent the percentage of cells with high HE staining (mean ± s.d; n = 4, $^{**}P < 0.01$, from THC-treated $Atg5^{+/+}$ MEFs).

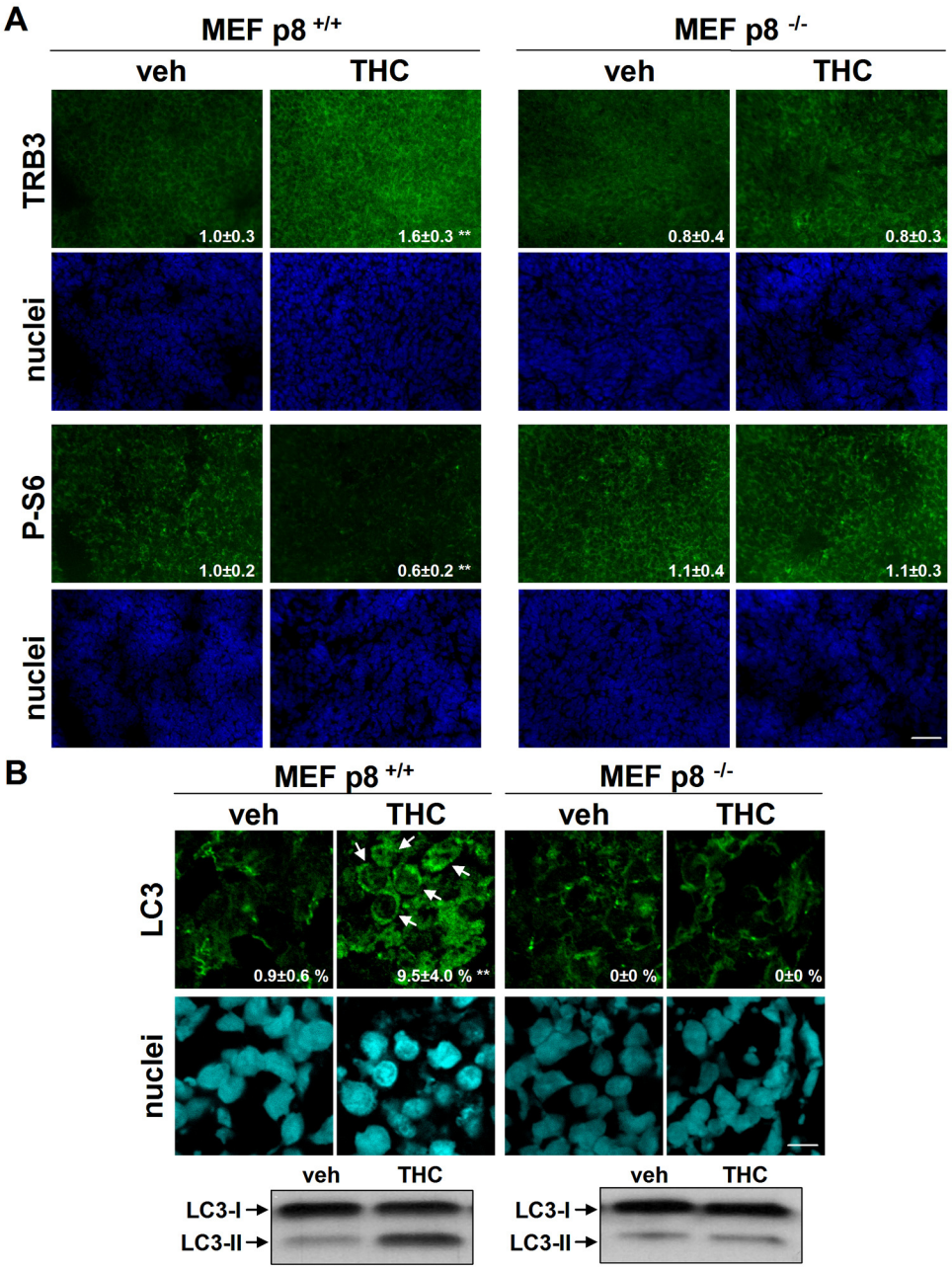

Supplemental Figure 10

THC activates the autophagy-mediated cell death pathway in $p8^{+/+}$ but not $p8^{-/-}$ xenografts. (**A**) Effect of THC administration on TRB3 and phospho-S6 immunostaining of Ras^{V12}/E1A-$p8^{+/+}$ and $p8^{-/-}$ tumor xenografts. Representative images of TRB3 and phospho-S6 immunostaining are shown. Values correspond to TRB3 or phospho-S6-stained area normalized to the total number of nuclei in each section and are expressed as the mean fold change ± s.d relative to vehicle-treated $p8^{+/+}$ tumors (18 sections for each of 3 dissected tumors for each condition were counted; $^{**}P < 0.01$ from vehicle-treated $p8^{+/+}$ tumors). Bar: 50 μm. (**B**) Upper panel: Effect of THC administration on LC3 immunostaining of Ras^{V12}/E1A-$p8^{+/+}$ and $p8^{-/-}$ tumor xenografts. Representative images of vehicle and THC-treated tumors are shown. Arrows point to cells with LC3 dots. Values correspond to the percentage of cells with LC3 dots relative to the total number of nuclei in each section ± s.d (10 sections for each of 3 dissected tumors for each condition were counted; $^{**}P < 0.01$ from vehicle-treated tumors). Bar: 20 μm. Lower panel: Effect of THC administration on LC3 lipidation of Ras^{V12}/E1A-$p8^{+/+}$ and $p8^{-/-}$ tumor xenografts. Representative samples from one vehicle and one THC-treated $p8^{+/+}$ and $p8^{-/-}$ tumors are shown.

Salazar et al. Supplemental Figure 10 (cont)

C

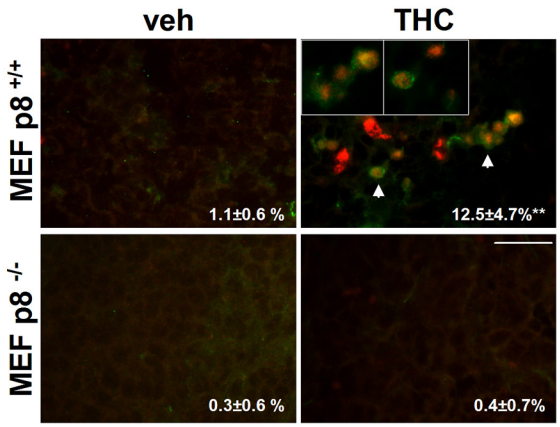

Supplemental Figure 10 (cont)
THC activates the autophagy-mediated cell death pathway in $p8^{+/+}$ but not $p8^{-/-}$ xenografts. (**C**) Effect of THC administration on active caspase-3 (red) and LC3 (green) immunostaining in Ras^{V12}/E1A-$p8^{+/+}$ and $p8^{-/-}$ MEF-tumor xenografts. Representative images from one vehicle and one THC-treated $p8^{+/+}$ and $p8^{-/-}$ tumors are shown. Values correspond to 10 sections of 3 dissected tumors for each condition and are expressed as the percentage of active caspase-3-positive cells relative to the total number of nuclei in each section (**$P < 0.01$ from vehicle-treated tumors). Bars: 20 μm.

Salazar et al. Supplemental Figure 11

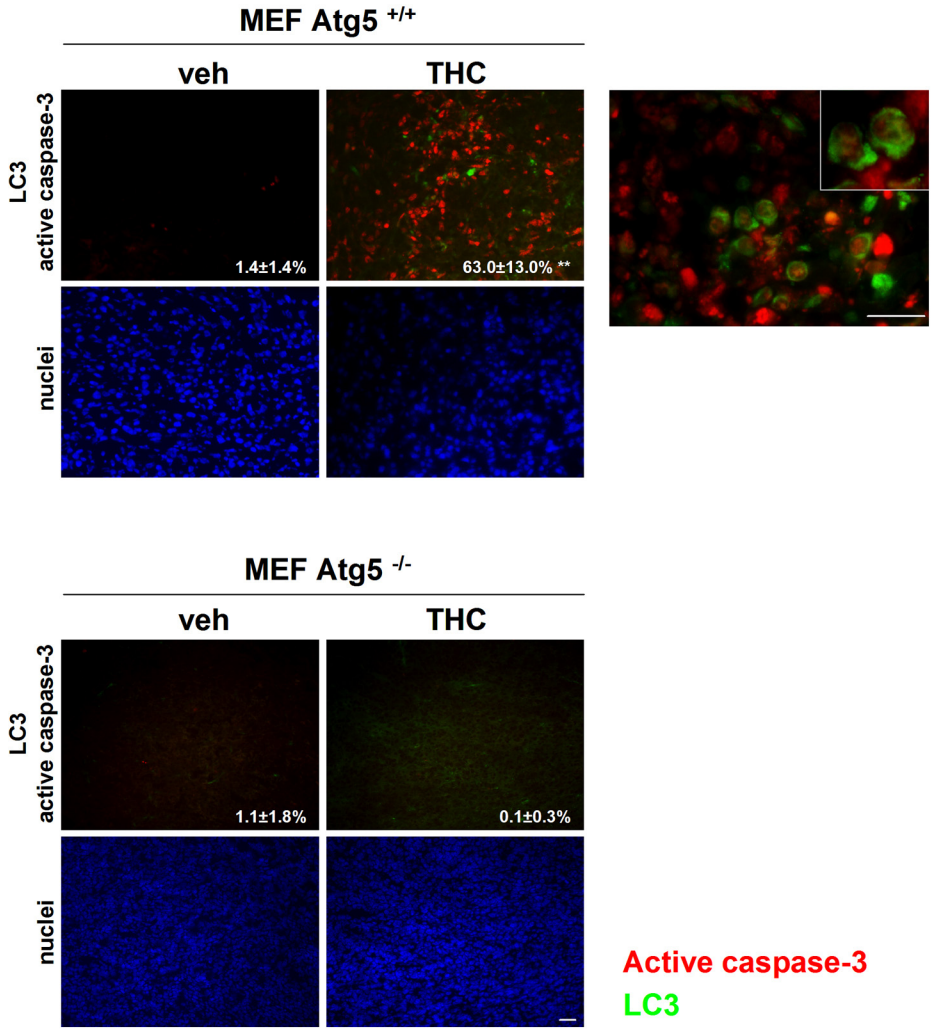

Supplemental Figure 11
THC activates the autophagy-mediated cell death pathway in $Atg5^{+/+}$ but not $Atg5^{-/-}$ xenografts. Effect of THC administration on active caspase-3 (red) and LC3 (green) immunostaining in T-large antigen/Ras^{V12}-$Atg5^{+/+}$ and $Atg5^{-/-}$ MEF-tumor xenografts. Representative images from one vehicle and one THC-treated $Atg5^{+/+}$ and $Atg5^{-/-}$ tumors are shown. A high magnification photomicrograph of a THC-treated $Atg5^{+/+}$ tumor is included (right panel). Values correspond to 10 sections of 3 dissected tumors for each condition and are expressed as the percentage of active caspase-3-positive cells relative to the total number of nuclei (**$P < 0.01$ from vehicle-treated tumors). Bars: 20 μm

Salazar et al. Supplemental Methods

Reagents. THC was from THC Pharm GmbH (Frankfurt, Germany), Z-VAD-FMK, pepstatin A, E64d and 3-methyl adenine (3-MA) were from Sigma (St. Louis, MO). Myriocin (ISP-1) was from Biomol (Plymouth Meeting, PA). Dolquine (hydroxychloroquine, HQ) was from Rubió Laboratorios (Barcelona, Spain).

Primary culture of brain tumor cells. The primary culture of brain tumor cells was obtained from biopsies donated by the Tumor Bank Network coordinated by the Spanish Cancer Research Centre. The human glioblastoma 14 (HG14) was diagnosed by the Pathology Department of Hospital Clínico San Carlos (Madrid, Spain). Tumor samples were homogenized, digested with type Ia collagenase (Sigma) for 1 h, and incubated on ice for 10 min. The supernatant was collected and, after centrifugation to discard the remaining death-floating cells, resuspended in DMEM containing 15% FBS. Finally, cells were seeded at a density of 400,000 cells/cm^2 and kept in culture for 2 weeks in DMEM containing 15% FBS and 1% glutamine.

Western blot and immunoprecipitation. Cells were lysed on a buffer containing 50 mM Tris HCl, pH 7.5, 1 mM phenylmethylsulfonyl fluoride, 50 mM NaF, 5 mM sodium pyrophosphate, 1 mM sodium orthovanadate, 0.1% Triton X-100, 1 μg/ml leupeptin, 1mM EDTA, 1 mM EGTA and 10 mM sodium β−glicerophosphate. For immunoprecipitation experiments, cells were lysed on a buffer containing 40 mM Hepes pH 7.5, 120 mM NaCl, 1mM EDTA, 10 mM sodium pyrophosphate, 10 mM sodium glycerophosphate, 50 mM sodium fluoride, 0.5 mM sodium orthovanadate and 0.3% CHAPS. Washes were performed with a kinase buffer containing 25 mM Hepes pH 7.5 and 50mM KCl. The following antibodies were used in this study: Anti- TRB3

antibody (1:5000; Abcam, Cambridge, UK) and anti-TRB3-aminoterminal end [ab50516 (Abcam), covalently coupled to IgG sepharose beads for IPs]; anti-phospho-eIF2a, anti-total S6 ribosomal protein, anti-phospho-S6 ribosomal protein Ser 235/236, anti total Akt, anti-phospho-Akt Ser473, anti-total p70 S6 kinase, anti-phospho-p70 S6 kinase Thr389, anti-phospho-TSC2 Thr 1462, anti-total TSC2 (1:1000; Cell Signaling Technology, Inc., Lake Placid, NY); anti-total PRAS40, anti-phospho-PRAS40 Thr246 antibodies (1:1000; kindly donated by Dr. Dario Alessi); anti-LC3 antibody (1:1000; polyclonal, MBL, Naka-Ku Nagoya, Japan, ref PM036); anti-alpha tubulin antibody (1:4000; Sigma).

RNA interference. Double-stranded RNA duplexes corresponding to human p8 (5'-GGAGGACCCAGGACAGGAU-3'), human TRB3 (5'-UCAUCUAAGAGAACCUAGGC-3'), human Ambra1 (5′-GGCCUAUGGUACUAACAAA-3′), human Atg1 (5'–CAGCAUCACUGCCGAGAGGUU-3'; 5'–CCACGCAGGUGCAGAACUAUU-3'; 5'–GCACAGAGACCGUGGGCAAUU-3'; 5'–UCACUGACCUGCUCCUUAAUU-3'), human Atg5 (5'-GGCAUUAUCCAAUUGGUUUUU-3'; 5'-GCAGAACCAUACUAUUUGCUU-3'; 5'-UGACAGAUUUGACCAGUUUUU-3'; 5'-ACAAAGAUGUGCUUCGAGAUU-3') and a non-targeted control (5'-UUCUCCGAACGUGUCACGU-3') were used.

Reverse transcription-PCR analysis. The following primers were used to amplify human p8 [5'-GAAGAGAGGCAGGGAAGACA-3' and 5'-CTGCCGTGCGTGTCTATTTA-3' (571 bp product)], human TRB3 [5'-GCCACTGCCTCCCGTCTTG-3' and 5'-GCTGCCTTGCCCGAGTATGA-3' (538 bp product)], rat TRB3 [5'-TGCCGCGCTTTTCCGACAGATG-3' and 5'-

TGCGGAGGAGACAGCGGATGAGG -3' (415 bp product)], human ATF-4 [5'-AGTCGGGTTTGGGGGCTGAAG-3' and 5'-TGGGGAAAGGGGAAGAGGTTGTAA-3' (436 bp poduct)], human CHOP [5'-GCGTCTAGAATGGCAGCTGAGTCATTGCC-3' and 5'-GCGTCTAGATCATGCTTGGTGCAGATTC-3' (508 bp product)], human Ambra-1 [5′- GGGCGAAATGCTCTACACCAA-3′ and 5′- CTCCGGCACCTCCCTCTCAGT-3′ (540 bp product)], human Atg5 [5′- TGGGCCATCAATCGGAACT-3′and 5′-CAAAAGGGTGACATGCTCTGATAA-3′ (560bp product)], human/mouse GAPDH [5'-GGGAAGCTCACTGGCATGGCCTTCC-3' and 5'-CATGTGGGCCATGAGGTCCACCAC-3' (322 bp product)]. PCR reactions were performed using the following parameters: 95ºC for 5 min, 94°C for 30 s, 52ºC (hTRB3), 55ºC (Ambra1), 57ºC (rTRB3) or 58°C (ATF-4, CHOP, p8, Atg5 and GAPDH) for 30s, and 72°C for 1 min, followed by a final extension step at 72°C for 5 min. The number of cycles was adjusted to allow detection in the linear range.

Real-time quantitative PCR. The following sense/antisense primers and probes were used for detecting human p8 (5′- CTATAGCCTGGCCCATTCCT-3′ and 5′-TCTCTCTTGGTGCGACCTTT-3′, probe 10), mouse p8 (5′-TTCCAGAACTCTGAAAGGAAAAA-3′ and 5′- GGTGTGGTGTCTGTGGTCTG-3′, probe 78), human TRB3 (5′- GTCTTCGCTGACCGTGAGA-3′ and 5′-CAGTCAGCACGCAGGAGTC-3′, probe 67), mouse TRB3 (5′-CGCTTTGTCTTCAGCAACTG-3′ and 5′-TCATCACGCAGGCATCTTC-3′, probe 67), human Atg1 (5′- TCATCTTCAGCCACGCTGT -3′ and 5′-CACGGTGCTGGAACATCTC -3′, probe 37), human Ambra1 (5′-CCCTCATTTCATTATCCCGTTA-3′ and 5′-GCGTAGTATGCAGCAGGAGA-3′, probe 15), human Atg5 (5′-CAACTTGTTTCACGCTATATCAGG-3′ and 5′-

CACTTTGTCAGTTACCAACGTCA-3′, probe 38), human ATF4 (5′-GGCCACCATGGCGTATTA -3′ and 5′- TGCTGAATGCCGTGAGAA -3′, probe 74), mouse ATF4 (5′- ATGGCGTATTAGAGGCAGCA-3′ and 5′-GCTGCTGGATTTCGTGAAG-3′, probe 74), human CHOP (5′-CAGAGCTGGAACCTGAGGAG -3′ and 5′- CTGCAGTTGGATCAGTCTGG -3′, probe 9), mouse CHOP (5′- ACCACCACACCTGAAAGCA-3′ and 5′-GACCTCCTGCAGATCCTCAT-3′, probe 11) and multi-species 18S RNA (GCTCTAGAATTACCACAGTTATCCAA and AAATCAGTTATGGTTCCTTTGGTC, probe 55). Amplifications were run in a 7900 HT-Fast Real-Time PCR System (Applied Biosystems). Each value was adjusted by using 18S RNA levels as reference.

Confocal microscopy. Cell cultures grown on 12 mm-coverslips were washed in PBS, fixed with 4% paraformaldehyde (20 min at room temperature) and permeabilized with 0.5% Triton X100 (5 min at room temperature) and incubated with the following primary antibodies (for 1 h at room temperature): rabbit polyclonal anti-PDI (1:100; Abcam, Cambridge, UK), rabbit polyclonal anti-cleaved caspase-3 Asp175 (1:100; Cell Signaling Technology), rabbit polyclonal anti-LC3 (1:200; MBL; refs: PM036 and PD014), or mouse monoclonal anti-LC3 antibody (1:100; Nanotools Antikörpertechnik GmbH & Co Antikörpertechnik GmbH & Co, Teningen, Germany; clone 5F10; for experiments shown in Figure 2 and 5A and staining of tumor xenografts). Incubation with appropriate Alexa-488 or Alexa-594-conjugated secondary antibodies (Invitrogen, Eugene, Oregon, USA) was performed in the dark at room temperature for 1 h. Cell nuclei were stained with Hoechst 33342 (Invitrogen). Finally, coverslips were mounted

in ProLong Gold antifade reagent (Invitrogen) and visualized in a Leica TCS SP2 confocal microscope.

Generation of tumor-promoting Atg5$^{+/+}$ and Atg5$^{-/-}$ MEFs. T-large antigen Atg5$^{+/+}$ and Atg5$^{-/-}$ cells were infected with supernatants obtained from Phoenix Ecotropic cells previously transfected with a retroviral-expressing vector encoding Ras^{V12} and a hygromycin resistance gene. Twenty resistant clones were selected, pulled and cultured in DMEM supplemented with 10% FBS.

Immunofluorescence from tumor samples. Samples from tumor xenografts were dissected and frozen. Samples from human tumors were fixed in 10% buffered formalin and then paraffin-embedded. After deparaffinization (only for human tumor samples) and fixation (only for samples from tumor xenografts), sections (5 μm) were permeabilized and blocked to avoid non-specific binding with 10% goat antiserum and 0,25% Triton X-100 in PBS for 45 min and subsequently incubated with mouse monoclonal anti-LC3 antibody (1:100; Nanotools Antikörpertechnik GmbH & Co; 4ºC, o/n), rabbit polyclonal anti-cleaved caspase-3 Asp175 (1:100; Cell Signaling Technology, Inc., Lake Placid, NY; 90 min, room temperature), rabbit polyclonal anti TRB3 (1:800; Calbiochem, San Diego, CA; 90 min, room temperature) or anti phospho S6 (1:200; Cell Signaling; 90 min, room temperature) antibodies, washed, further incubated with the corresponding Alexa-488 or Alexa-594-conjugated secondary antibodies (Invitrogen; 90 min, room temperature) and mounted with Mowiol mounting medium (Merck, Darmstadt, Germany) containing TOTO-3 iodide (Molecular Probes, U87MG tumor xenografts and human samples). Nuclei from MEF-derived tumor

xenografts were stained with Hoechst 33342 (Invitrogen; 10 min, room temperature) before montage with Mowiol was performed.

Immunohistochemistry from human tumor samples. Samples from human tumors were fixed, paraffin-embedded and processed as described in the previous point. Sections were incubated with monoclonal anti-LC3 antibody (1:100; Nanotools Antikörpertechnik GmbH & Co) or with anti-cleaved caspase-3 Asp175 (1:100; Cell Signaling Technology), followed by incubation with a secondary anti-IgG biotinylated antibody (Vector laboratories, Burlingame, CA). Detection was performed with DAB Peroxidase Substrate kit (Vector laboratories) and the slides were counterstained with hematoxylin (Fisher Scientific, Pittsburgh, PA) and mounted in xylene-based mounting media.

Processing of samples for electron microscopy. Cell monolayers were fixed with a mixture of 2% glutaraldehyde and 1% tannic acid in 0.4 M HEPES buffer (pH 7.4) for 1 h at room temperature. Fixed cells were removed from the culture dishes in the fixative, washed with HEPES buffer, and treated with a mixture of 1% osmium tetroxide and 0.8% potassium ferricyanide in distilled water (1 h at 4°C), followed by an incubation with 2% uranyl acetate. Finally, cells were dehydrated in increasing concentrations of acetone (50, 70, 90, and 100%) for 15 min each at 4°C and embedded by conventional procedures in the epoxy-resin EML-812.